minerals

MDPI

Article

# Study on Selective Removal of Impurity Iron from Leached Copper-Bearing Solution Using a Chelating Resin

**Yubiao Li [1,2,3,*], Xinyu Wang [1], Qing Xiao [3] and Xu Zhang [4]**

1 School of Resources and Environmental Engineering, Wuhan University of Technology, Wuhan 430070, China; wxy1992125@163.com
2 Hubei Key Laboratory of Mineral Resources Processing and Environment, Wuhan 430070, China
3 School of Natural and Built Environments, University of South Australia, Mawson Lakes, SA 5095, Australia; qing.xiao@mymail.unisa.edu.au
4 Hubei Environmental Monitoring Centre, Wuhan 430072, China; jidingzhi@yeah.net
* Correspondence: Yubiao.Li@whut.edu.cn

Academic Editor: Saeed Chehreh Chelgani
Received: 3 September 2016; Accepted: 8 October 2016; Published: 15 October 2016

**Abstract:** In order to selectively remove iron from copper laden solution after leaching but prior to electrowinning, equilibrium, kinetic, and thermodynamic studies have been conducted on an a chelating resin of Rexp-501 at pH 1.0 and at various temperatures. Both Langmuir and Freundlich models were investigated, with the Langmuir model proving to be more suitable for fitting iron removal performance, with little influence from copper concentration. Compared with the pseudo first order kinetic model, the pseudo second order kinetic model fitted the dynamic adsorption process better, indicating a chemisorption mechanism. Fourier transform infrared spectroscopy (FT-IR) results indicated that C=O from carbonyl group played a key role in combining with iron and can be regenerated and reused. However, the C=O of the acylamino group combining with iron was not able to be released after oxalic acid was applied.

**Keywords:** separation; chelating resin; adsorption isotherms; regeneration

## 1. Introduction

The hydrometallurgical processing of copper-bearing minerals has attracted much attention due to its relatively cost-effective and environmentally friendly properties as compared with its pyrometallurgical counterpart [1–5]. Due to the complexity of the naturally formed minerals, leaching of other gangue-containing impurity elements or minerals normally accompanies the dissolution of copper minerals, resulting in the significant release of some cations, especially iron that dissolved remarkably with copper from the copper-iron minerals such as chalcopyrite. As chalcopyrite accounts for approximately 70% of the copper reserve worldwide [6,7], the separation of these cations from copper pregnant solutions is a key step for successful copper enrichment. Most studies have tried to recover the valuable copper using solvent extraction [8–11]. However, less attention has been paid to removing the impurity cations, especially the great amount of iron present in the laden solution, thereby leaving a much purer copper solution. As the chalcopyrite leaching solution containing impure iron would lead to a problem for the subsequent extraction of copper in the electrowinning process, the separation of iron from copper-bearing solutions obtained in the hydrometallurgical process of copper-containing minerals such as chalcopyrite [2,5] is of great concern worldwide.

The simplest way to remove iron is to add chemicals to increase the solution pH to precipitate iron. However, the precipitated solution with high pH values should be treated with acid again prior to reusing for further chalcopyrite leaching. Therefore, the techniques having the capability

to remove iron but not increasing solution pH are desired in the hydrometallurgical processing of copper minerals, especially at low pH conditions that are suitable for acid leaching. Considering the technologies applied in, e.g., wastewater treatment, many adsorbents used in heavy metal removal from wastewater, such as activated carbon [12], graphite oxide [13], ion-exchange [14], and membrane technologies [15], have been applied to treat heavy metals in wastewater, although some industrial byproducts have also been utilized for heavy metal treatments [16–18].

Recently, the selective adsorption strategy using chelating resins has been paid enormous attention due to its simplicity, high efficiency, and low cost during the adsorption processes [19–21]. Polymerization of conventional chelating monomers such as acrylic acid, methacrylic acid, and vinylpyridine has been extensively investigated to develop suitable resins to selectively adsorb metal ions [22–25]. This study was therefore aimed to investigate the selective removal capability of iron by a chelating resin at a low pH condition. In addition, the regeneration capacity of the resin was also investigated.

## 2. Materials and Methods

### 2.1. Chemicals

The chelating resin Rexp-501 was purchased from Ruilekang Separation Technology, Beijing, China. The size of the white spherical resin ranges from 178 to 840 μm. The inorganic and organic chemicals including $CuSO_4$, $Fe_2(SO_4)_3$, $H_2SO_4$, HCl, oxalic acid ($C_2H_2O_4$), and citric acid ($C_6H_8O_7$) were of analytical grade and purchased from Sinopharm Chemical Reagent Co., Ltd., Shanghai, China. In addition, KBr used for Fourier transform infrared spectroscopy (FT-IR) analysis was in spectral purity. All chemicals were used as received without any modification.

### 2.2. Adsorption Experiment

All adsorption experiments were carried out using fresh solutions prepared from analytical grade reagents and MilliQ water with a resistivity greater than 18.2 MΩ·cm. Iron loading solutions of various concentrations (170–10,000 $mg \cdot L^{-1}$) were prepared using ferric sulfate ($Fe_2(SO_4)_3$), with pH being adjusted to 1.0 using $H_2SO_4$. For the iron adsorption experiment in the presence of copper, a mixture containing both copper using $CuSO_4$ and iron using $Fe_2(SO_4)_3$ was synthesized.

For the adsorption experiment, 1–50 g Rexp-501 was added into 100 mL solutions with various iron and copper concentrations and shaken in an air bath oscillator at 298–328 K and 150 rpm. In addition, the kinetic studies were sampled at a reasonable interval (i.e., 0.5, 1, 2, 3, 4, 5, 8, 10, 15, 20, 30, 60, and 90 min). After adsorption, a 1 mL solution was taken out for a solution assay.

The amount of iron or copper adsorbed by Rexp-501 was determined according to Equation (1):

$$Q_e = \frac{C_0 V_0 - C_e V_e}{W}, \quad (1)$$

where $Q_e$ is the amount of iron or copper adsorbed per unit weight of Rexp-501, $C_0$ and $C_e$ are the iron concentrations before and after adsorption, and $V_0$ and $V_e$ are the volumes of the solution before and after adsorption, respectively. $W$ is the weight of the chelating resin added to the solution.

The regeneration experiments were conducted using 10 wt % various acids (Sections 2.1 and 3.6, i.e., $H_2SO_4$, HCl, $C_2H_2O_4$, and $C_6H_8O_7$) to remove ions from saturated resin. After being generated in such a way, the resin was further used to test its adsorption capacity.

### 2.3. Measurements

The element concentrations were analyzed using a flame atomic absorption spectroscopy Agilent AA240FS (Agilent Technologies Inc., Santa Clara, CA, USA), while the functional groups of this resin were analyzed via Fourier transform infrared spectroscopy (FT-IR, Nicolet IS10, Thermo Fisher, Waltham, MA, USA). All the FT-IR samples were prepared mixed with spectral purity KBr (150 mg) and resin (1 mg), and pressed to form pellets prior to analysis.

## 3. Results and Discussions

### *3.1. Separation Efficiency*

The synthetic solution with both iron and copper added at the same time were treated by a chelating resin named Rexp-501 to evaluate its separation efficiency of iron from copper solutions. Figure 1 shows the adsorption amounts of iron and copper under various concentrations, but under a constant temperature of 298 K. It is observed that the unit adsorption capacity for iron decreased gradually from 3.53 to 1.86 mg/g when the resin amount increased from 1 to 6 g/100 mL, but that for copper remained lower than 0.13 mg·L$^{-1}$ when iron and copper concentrations were both 170 mg·L$^{-1}$. When iron and copper concentrations increased from 170 to 680 mg·L$^{-1}$, the adsorption capacity of iron increased significantly, but that of copper did not follow the same trend, indicating that better separation efficiency of iron from copper-containing solutions can be achieved at greater iron and copper concentrations. This further verified that resin Rexp-501 is capable of separating iron from copper solutions at high concentrations.

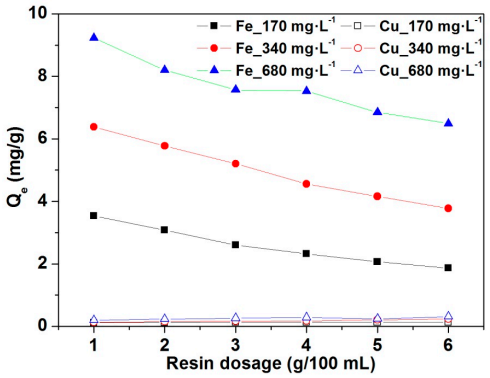


**Figure 1.** Iron and copper adsorption by Rexp-501 at various concentrations, 298 K.

Furthermore, Figure 2 shows the separation efficiency (iron and copper) of iron from copper solutions using the same concentration as shown in Figure 1. As indicated, the separation efficiency decreased gradually when the resin amount increased. However, the ratio between the adsorption amount of iron and copper increased when iron and copper concentrations increased from 170 to 680 mg·L$^{-1}$, indicating that greater iron and copper concentrations resulted in better iron and copper separation. This is very important in separating iron from chalcopyrite leaching solution in industry, as both copper and iron concentration were very high prior to the separation or extraction step. The above results indicated that the adsorption of iron was not influenced by the copper concentration, as the adsorption of copper was limited to a very low level. Therefore, further studies will only focus on the adsorption of iron in the absence of copper.

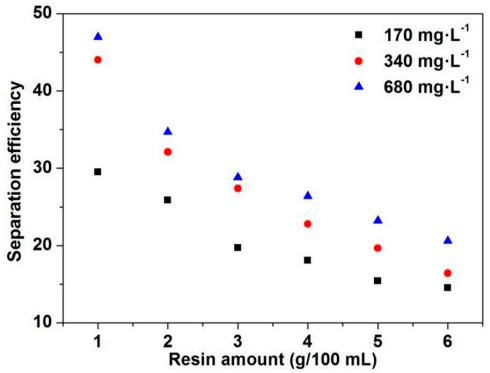


**Figure 2.** Separation efficiency (iron-to-copper ratio) by Rexp-501 at various concentrations, 298 K. Copper and iron in the same concentrations.

### 3.2. Effects of Resin Amount

Figure 3 summarizes the removal efficiency of iron from synthetic solution with different iron concentrations (170–10,000 mg·L$^{-1}$) using Rexp-501 at 298 K and 150 rpm for 90 min. As indicated, the iron removal percentage increased with the resin amount increased. Specifically, when the resin dosage was 10 g/100 mL, there was a significantly different iron adsorption under various iron concentrations, e.g., over 95% of iron was adsorbed when iron concentration was lower than 680 mg·L$^{-1}$. However, when iron concentration increased to 1700 mg·L$^{-1}$, only approximately 80% of the iron was removed, with the removal efficiency being further reduced when iron concentration increased, e.g., achieving less than 30% of iron removal when iron concentration was 10,000 mg·L$^{-1}$. It should be noted that the final removal of iron was almost 100% for all conditions when a sufficient amount of resin was added.

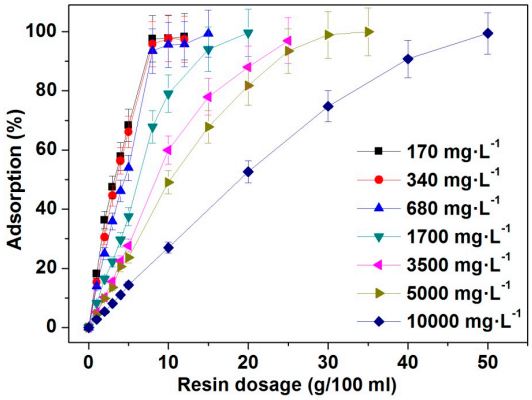


**Figure 3.** Iron adsorption by resin Rexp-501 at pH 1.0, 298 K and 150 rpm for 90 min.

Furthermore, Figure 4 shows that the iron adsorption capacities of Rexp-501 decreased linearly as a function of resin dosage at any iron concentration. However, iron removal capacity increased when iron concentration increased, e.g., from approximately 3 mg·g$^{-1}$ at 170 mg·L$^{-1}$ to more than 30 mg·g$^{-1}$ at 10,000 mg·L$^{-1}$, indicating that sufficient utilization of resin and optimized iron removal rate were available at greater iron concentrations.

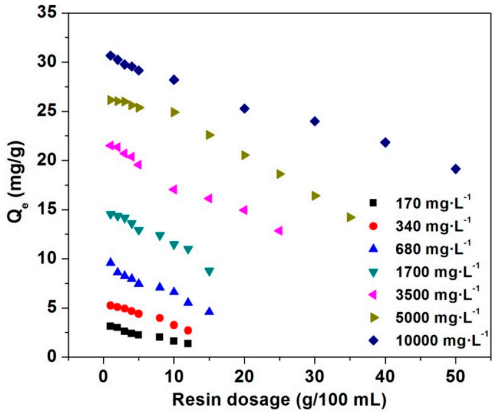


**Figure 4.** Iron adsorption capacity of resin Rexp-501 at various iron concentrations, 298 K.

### 3.3. Adsorption Isotherms

Adsorption isotherms reveal the relationship between the equilibrium adsorption quantity and the equilibrium concentration ($C_e$) under a certain temperature. Both Langmuir (Equation (2)) and Freundlich (Equation (3)) equations were applied to fit the isothermal data:

$$\frac{C_e}{Q_e} = \frac{C_e}{Q_m} + \frac{1}{bQ_m}, \text{ and} \quad (2)$$

$$\log Q_e = \log K_f + \frac{1}{n}\log C_e, \quad (3)$$

where $Q_e$ is the amount of adsorption per unit mass of sorbent, $C_e$ is the equilibrium concentration of iron in the solution, $Q_m$ is the amount of adsorbate at complete monolayer coverage, and $b$ is the Langmuir isotherm constant related to the energy of adsorption. $K_f$ and $1/n$ are Freundlich constants related to the adsorption capacity and intensity, respectively.

The Langmuir and Freundlich isothermal fitting results are shown in Figure 5 and Table 1. It is evident that the adsorption capacity of this resin fitted the experimental results well at any concentration investigated using the Langmuir isotherm model, e.g., increasing from approximately 3 mg·g$^{-1}$ at 170 mg·L$^{-1}$ to more than 30 mg·g$^{-1}$ at 10,000 mg·L$^{-1}$. In contrast, the isotherm constant $b$ decreased from 0.1288 to 0.0021 when iron concentration increased from 170 to 10,000 mg·L$^{-1}$.

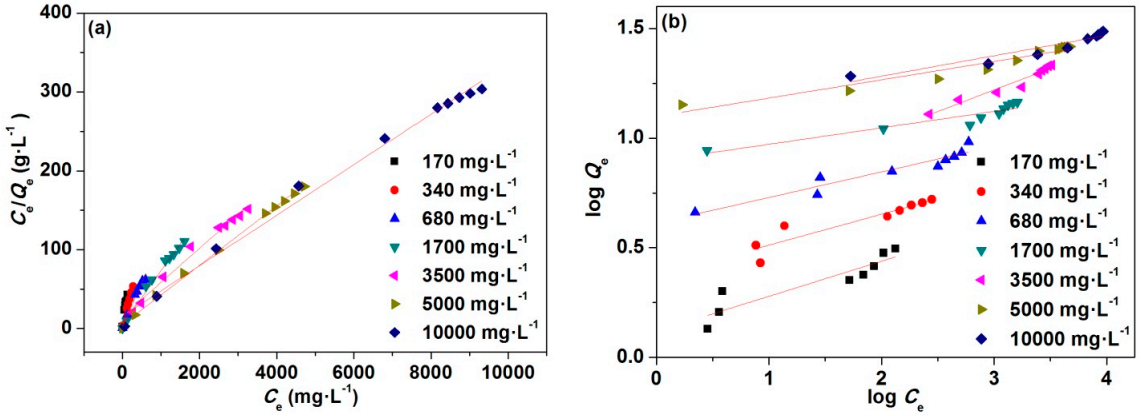


**Figure 5.** (**a**) Langmuir and (**b**) Freundlich isotherms of iron adsorption by Rexp-501 at 298 K.

**Table 1.** Fitting results of Langmuir and Freundlich isotherms ($R^2$ is the correlation of determination).

| Concentration (mg·L$^{-1}$) | Langmuir Isotherm | | | | Freundlich Isotherms | | |
|---|---|---|---|---|---|---|---|
| | $Q_m$ (exp) (mg·g$^{-1}$) | $Q_m$ (cal) (mg·g$^{-1}$) | $b$ (L·mg$^{-1}$) | $R^2$ | $K_f$ | $1/n$ | $R^2$ |
| 170 | 3.1273 | 3.0562 | 0.1288 | 0.9655 | 1.3152 | 0.1598 | 0.8169 |
| 340 | 5.2458 | 5.2604 | 0.1020 | 0.9946 | 2.3496 | 0.1409 | 0.8369 |
| 680 | 9.5836 | 9.0580 | 0.0401 | 0.9806 | 4.0986 | 0.1167 | 0.9102 |
| 1700 | 14.5470 | 14.6628 | 0.0132 | 0.9861 | 7.8864 | 0.0749 | 0.8714 |
| 3500 | 21.5379 | 23.1481 | 0.0098 | 0.9838 | 4.2565 | 0.1969 | 0.9447 |
| 5000 | 26.1574 | 26.5957 | 0.0077 | 0.9977 | 12.5707 | 0.0831 | 0.9316 |
| 10,000 | 30.6689 | 31.2500 | 0.0021 | 0.9919 | 12.4825 | 0.0930 | 0.8924 |

As $1/n < 1$ indicates favorable adsorption while $1/n > 1$ suggests cooperative adsorption, these $1/n$ values shown in Table 1 revealed that iron adsorption by Rexp-501 was favorable [26]. The $K_f$ values varied but had a generally increasing trend with increasing iron concentration, indicating that greater adsorption capacity may be achievable at higher iron concentrations. However, as compared with the $R^2$ values obtained from Langmuir model fitting (greater than 0.96, Table 1), all the $R^2$ values calculated from the Freundlich model was lower, suggesting that the Langmuir model was more appropriate than the Freundlich model, and iron was adsorbed in a monolayer coverage status on the resin.

### *3.4. Thermodynamic Analysis*

As shown in Figure 3, the addition of 25 g of resin can result in a 90% iron removal when iron concentration was 5000 mg·L$^{-1}$, further thermodynamic analysis was conducted to investigate the temperature effect. As shown in Figure 6, the iron adsorption process had three stages. Within the initial 6 min, a linear and rapid increase in iron removal by adsorption was observed, followed by a gradual increase until 30 min. The adsorption tended to be equivalent after 60 min, indicating a rapid adsorption resin [27]. It should be noted that the iron adsorption by resin varied insignificantly when

temperature increased from 298 to 328 K within 6 min, but over 60% of iron was adsorbed within this period. In the following adsorption stage, the iron adsorption rate increased gradually with the increased temperature, although the final removal of iron (approximately 95%) was almost the same at 90 min, achieving a $Q_e$ ranging from 18.43 to 18.74 mg·g$^{-1}$ from 298 to 328 K.

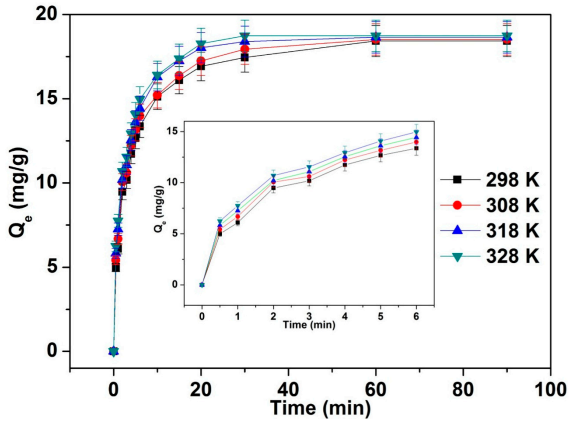


**Figure 6.** Iron adsorption by resin Rexp-501 at iron concentrations of 5000 mg·L$^{-1}$.

### *3.5. Adsorption Kinetics*

To further analyze the adsorption kinetics, the Lagergren pseudo first order [28] and second order [29,30] equations (Equations (4) and (5), respectively) were applied in the modeling iron adsorption on this resin.

$$\log (Q_e - Q_t) = \log Q_e - \frac{k_1 t}{2.303}; \quad (4)$$

$$\frac{t}{Q_t} = \frac{1}{k_2 Q_e^2} + \frac{t}{Q_e}; \quad (5)$$

here, $Q_e$ (mg·g$^{-1}$) is the equilibrium concentration of iron on resin, and $Q_t$ (mg·g$^{-1}$) is the amount of iron adsorbed on resin at time $t$. $k_1$ (min$^{-1}$) and $k_2$ (g·mg$^{-1}$·min$^{-1}$) are the rate constants for the pseudo first order and pseudo second order equations, respectively. It should be noted that only the data collected within 30 min were used to fit the model, as there were no significant improvements in the adsorption at 60 or 90 min. Figure 7 shows the fitting of data shown in Figure 6, but restricted to the fast adsorption stage, i.e., the first 30 min, within which nearly 100% iron removal was achieved at 328 K.

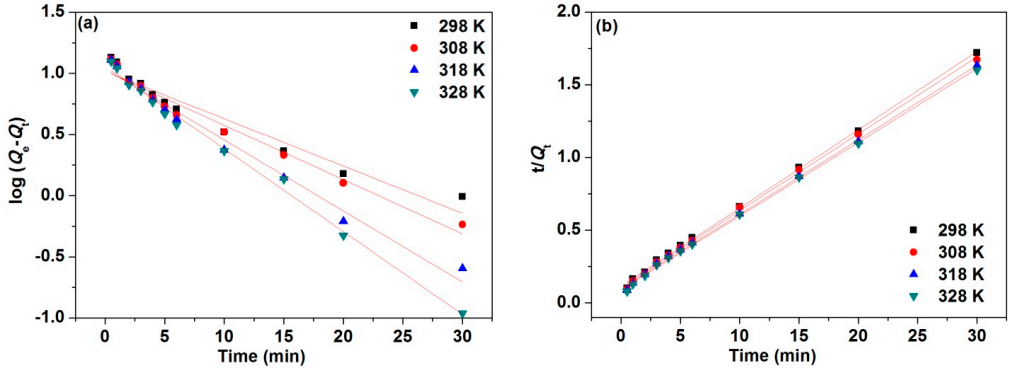


**Figure 7.** Fittings of iron adsorption by Rexp-501. (**a**) Lagergren pseudo first order model; (**b**) Lagergren pseudo second order model.

As shown in Table 2, the equilibrium adsorption capacities using the Lagergren pseudo first order model differs from that observed experimentally at all temperatures tested (Figure 6 and Table 2),

indicating that this model is not suitable for modeling the adsorption process. However, the $Q_e$ calculated based on the Lagergren pseudo second order are very close to that derived from the experiment. In addition, all the $R^2$ values are greater than 0.998, indicating that the adsorption of iron by Rexp-501 follows the Lagergren pseudo second order kinetic model. This further confirms that iron adsorption by resin Rexp-501 is due to chemisorption [31].

**Table 2.** Lagergren pseudo first and second order kinetics parameters for iron adsorption by resin Rexp-501.

| $T$ (K) | First Order | | | | Second Order | | | |
|---|---|---|---|---|---|---|---|---|
| | $Q_e$ (exp, mg·g$^{-1}$) | $k_1$ (min$^{-1}$) | $Q_e$ (mg·g$^{-1}$) | $R^2$ | $k_2$ (g·min$^{-1}$·mg$^{-1}$) | $Q_e$ (mg·g$^{-1}$) | $t_{1/2}$ (min) | $R^2$ |
| 298 | 18.43 | 0.0888 | 10.3412 | 0.9342 | 0.0253 | 18.5908 | 2.1257 | 0.9987 |
| 308 | 18.52 | 0.1020 | 10.4323 | 0.9683 | 0.0263 | 18.9322 | 2.0112 | 0.9983 |
| 318 | 18.65 | 0.1336 | 10.8665 | 0.9815 | 0.0267 | 19.5389 | 1.9134 | 0.9987 |
| 328 | 18.74 | 0.1557 | 11.4583 | 0.9926 | 0.0281 | 19.7472 | 1.8021 | 0.9987 |

The half-adsorption time, $t_{1/2}$, as the time for half of the adsorbate adsorbed on the adsorbent, is often used as a measure of the adsorption rate (Equation (6)):

$$t_{1/2} = \frac{1}{k_2 Q_e}. \quad (6)$$

The $t_{1/2}$ values were present in Table 2. With the increase in temperature from 298 to 328 K, the half-adsorption time decreased gradually, from 2.1257 to 1.8021 min. The fast adsorption rate in the initial stage was probably due to the availability of a large number of chelating sites.

As the pseudo second order model fitted the adsorption process well, the rate constant $k_2$ was used to calculate the adsorption energy of activation using the Arrhenius equation (Equation (7)):

$$\ln k_2 = -\frac{E_a}{2.303RT} + \text{constant}, \quad (7)$$

where $k_2$ is the rate constant (g), $R$, $E_a$, and $T$ are gas constant (8.314 J·mol$^{-1}$·K$^{-1}$), energy of activation (kJ·mol$^{-1}$), and the temperature in Kelvin, respectively. $E_a$ can be calculated via the plot of ln$k_2$ against 1000/T (Figure 8). The activation energy for iron adsorption was found to be 6.16 ± 0.93 kJ·mol$^{-1}$, indicating that the adsorption was determined by a diffusion controlled process rather than a chemical reaction mechanism [6,32].

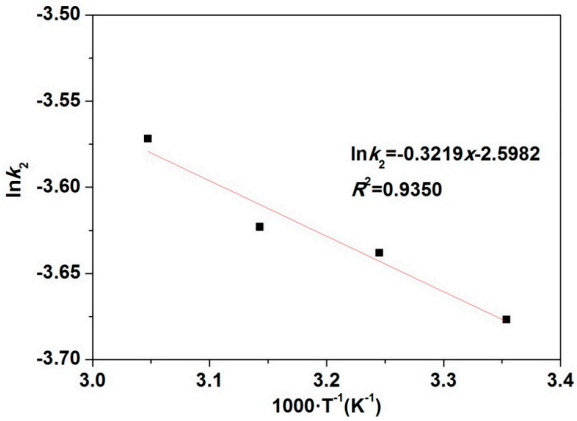


**Figure 8.** Arrhenius plot for iron adsorption by Rexp-501.

### *3.6. Regeneration and Reuse*

In order to investigate the regeneration capacity of Rexp-501, the saturated resins were further desorbed using four acids, i.e., $H_2SO_4$, HCl, oxalic acid, and citric acid. Figure 9 showed that more

than 60% iron was removed by adding 10 wt % acids given above, except for citric acid. It is evident that the highest removal efficiency was achieved when oxalic acid was added, following by HCl and then $H_2SO_4$, with citric acid being the lixivant with the lowest iron removal efficiency (less than 40%).

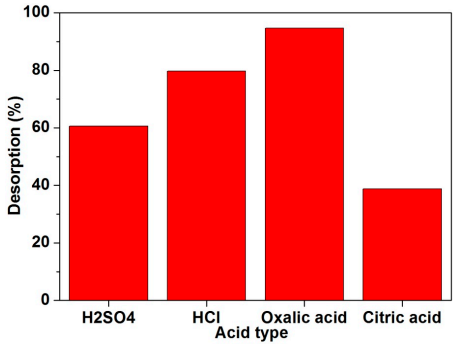


**Figure 9.** The effects of acid type on iron removal from saturated Rexp-501, 298 K.

Further desorption kinetic studies by oxalic acid (Figure 10) demonstrated that iron can be removed very quickly, e.g., approximately 90% of the iron was removed within the initial 5 min. However, in the following 15 min, iron removal increased gradually, achieving a 94.6% removal at the end of 20 min, which was further increased to 99.8% when an additional 10 mL oxalic acid solution was applied after filtration (data not shown in Figure 10). The greater iron removal was achieved when the second desorption solution was used, probably due to the equilibrium of iron in the first desorption solution.

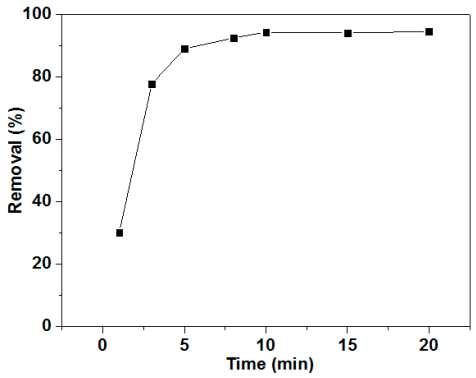


**Figure 10.** Iron desorption kinetics by oxalic acid.

The regenerated resin was further used to adsorb iron solution with a concentration of 5000 mg·L$^{-1}$ to study its reusability. The results showed that the unit capacity of the regenerated Rexp-501 was 14.63 mg·g$^{-1}$, lower than 19.58 mg·g$^{-1}$ of the fresh resin sample, indicating that a portion of the metal adsorption capacity of Rexp-501 was lost, probably due to the reduced amount of functional groups on the resin surface that cannot be released from bonded iron via acid treatment. It should be noted that the capacity of 14.63 mg·g$^{-1}$ lasted for at least 10 times in the manner of use and regeneration using oxalic acid, indicating a good capacity of regeneration.

### *3.7. Adsorption Mechanisms*

The adsorption mechanism can be determined through themodynamic parameters such as enthalpy ($\Delta H$), entropy ($\Delta S$), and free energy ($\Delta G$), according to Equations (8)–(11):

$$K_c = \frac{C_{Ae}}{C_e}, \quad (8)$$

$$\Delta G = -RT\ln K_c, \tag{9}$$

$$\ln K_c = \frac{\Delta S}{R} - \frac{\Delta H}{RT}, \text{ and} \tag{10}$$

$$\Delta G = \Delta H - T\Delta S \tag{11}$$

where $K_c$ is the thermodynamic equilibrium constant, and $C_{Ae}$ and $C_e$ are the adsorbed and equilibrium concentrations of iron in the solution. $\Delta G$ is the free energy of adsorption (J·mol$^{-1}$), $T$ is the temperature in Kelvin, $R$ is the universal gas constant, which is 8.314 J·mol$^{-1}$·K$^{-1}$, $\Delta H$ is the heat of adsorption, and $\Delta S$ is the standard entropy change. The $\Delta H$ (8122.78 J·mol$^{-1}$) and $\Delta S$ (49.31 J·mol$^{-1}$·K$^{-1}$) values can be obtained from the slope and intercept of a plot of ln$K_c$ against $1/T$. The thermodynamic parameters are shown in Table 3.

**Table 3.** The thermodynamic parameters.

| $T$ (K) | $\Delta G_{(exp)}$ (J·mol$^{-1}$) | $\Delta G_{(cal)}$ (J·mol$^{-1}$) | $K_c$ |
|---|---|---|---|
| 298 | −6613.66 | −6588.58 | 14.4121 |
| 308 | −7036.82 | −7081.67 | 15.5904 |
| 318 | −7582.72 | −7574.75 | 17.5790 |
| 328 | −8078.50 | −8067.84 | 19.3186 |

The negative $\Delta G$ value indicated that the adsorption of iron was a spontaneously occurring process at all temperatures. The value of $\Delta G$ were more negative when temperatures increased, indicating greater efficient adsorption at greater temperature. The positive $\Delta H$ and increased $K_c$ values with the increased temperatures indicated that the adsorption of iron was an endothermic process [32].

Figure 11 demonstrates the FT-IR spectra of the fresh and iron adsorbed resins at 298 and 328 K as well as the resin desorbed using oxalic acid for 20 min at 298 K. The adsorption at 1733 cm$^{-1}$ in Figure 11a indicates the presence of ester carbonyl groups (C=O) due to stretching vibration [33,34]. A strong peak at 1655 cm$^{-1}$ was ascribed to the stretching vibrations of C=O in acylamino groups [33], while the peak at 1406 cm$^{-1}$ was ascribed to C–N stretching vibration [35]. In addition, the peak at 1451 cm$^{-1}$ suggested the deformation vibrations of metal hydroxyl groups and interstitial water ($\delta_3$ (M–OH) + $H_2O$ inters) [36].

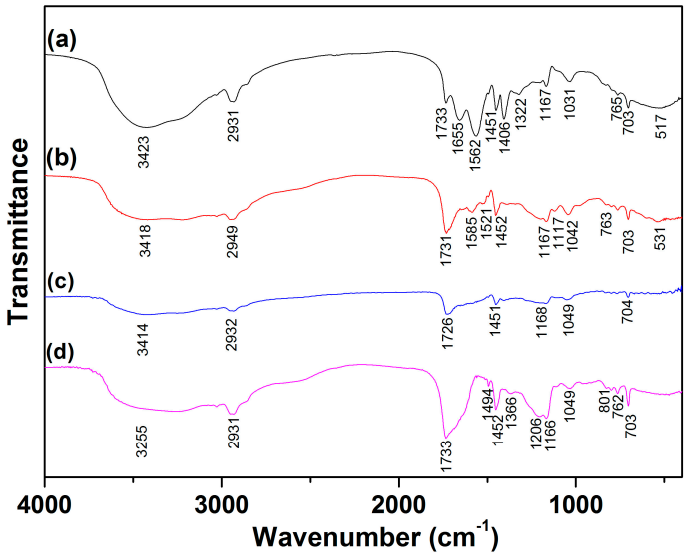


**Figure 11.** FT-IR spectra of fresh and adsorbed resins. (**a**) Fresh; (**b**) adsorbed at 298 K; (**c**) adsorbed at 328 K; (**d**) desorbed using oxalic acid at 298 K.

When iron was adsorbed at 298 and 328 K (Figure 11b,c, respectively), the peaks of ester carbonyl groups shifted to 1731 and 1726 cm$^{-1}$, respectively, indicating the adsorption of iron with the –COO$^-$

group, which was further confirmed by the desorbed resin shown in Figure 11d where a peak at 1733 $cm^{-1}$ is present again. The further shift observed at 328 K indicated that more iron was adsorbed by the carbonyl functional groups. The presence of 1733 $cm^{-1}$ observed in the desorbed resin (Figure 11d), which can be further used to adsorb metal gain (Section 3.6), indicated that the stretching vibration of the ester carbonyl groups played an important role in iron adsorption and can be regenerated after acid leach. However, the functional groups at 1655 $cm^{-1}$ disappeared after adsorption (Figure 11b,c, respectively) and regeneration (Figure 11d, respectively), suggesting that the stretching vibrations of the $H_2N$=C=O group cannot be regenerated after oxalic acid leach. Therefore, the functional groups can be reused in the iron adsorption due to the presence of ester carbonyl groups (C=O) on the Rexp-501 surface.

## 4. Conclusions

The present study shows that the chelating resin Rexp-501 is an effective adsorbent for the selective removal of iron from copper-containing solutions. Iron adsorption follows both Langmuir isotherm and pseudo second order kinetic models, indicating that iron adsorption by Rexp-501 follows a chemisorption mechanism. In addition, this resin adsorbs iron in a very fast manner. The adsorption capacity of iron via Rexp-501 increases with increased temperature, and further thermodynamic analysis indicates a spontaneous and endothermic adsorption process. Most of the iron adsorbed on the saturated resin is successfully removed by various acids, with oxalic acid being the most effective agent. Moreover, after 10-fold regeneration and reuse, the resin still presents good capacity for iron removal, with a portion of the iron removal capacity being lost. FT-IR analysis indicates that this portion is probably due to the $H_2N$=C=O group that cannot be released after combining with iron. In contrast, the ester carbonyl groups (C=O) have a more important role in removing iron and can be regenerated and reused. Further studies can be focused on the quantity identification of these functional groups.

**Acknowledgments:** This work is financial supported by the National Natural Science Foundation of China under the project No. 51604205 and the support from Fundamental Research Funds for the Central Universities (WUT: 2016IVA046) is also gratefully acknowledged.

**Author Contributions:** Yubiao Li and Xinyu Wang conceived and designed the experiments; Yubiao Li, Xinyu Wang and Qing Xiao analyzed data, Yubiao Li and Xu Zhang conducted calculations. All authors have contributed to the discussion and writing of the paper.

**Conflicts of Interest:** The authors declare no conflicts of interest.

## References

1. Li, Y.; Qian, G.; Li, J.; Gerson, A.R. Kinetics and roles of solution and surface species of chalcopyrite dissolution at 650 mV. *Geochim. Cosmochim. Acta* **2015**, *161*, 188–202. [CrossRef]
2. Li, Y.; Wei, Z.; Qian, G.; Li, J.; Gerson, A. Kinetics and mechanisms of chalcopyrite dissolution at controlled redox potential of 750 mV in sulfuric acid solution. *Minerals* **2016**, *6*, 83. [CrossRef]
3. Dong, C.L.; Mattesini, M.; Augustsson, A.; Wen, X.G.; Zhang, W.X.; Yang, S.H.; Persson, C.; Ahuja, R.; Lüning, J.; Chang, C.L.; et al. Electronic structure and surface structure of $Cu_2S$ nanorods from polarization dependent X-ray absorption spectroscopy. *J. Electron Spectrosc. Relat. Phenom.* **2006**, *151*, 64–70. [CrossRef]
4. Majuste, D.; Ciminelli, V.S.T.; Osseo-Asare, K.; Dantas, M.S.S.; Magalhães-Paniago, R. Electrochemical dissolution of chalcopyrite: Detection of bornite by synchrotron small angle X-ray diffraction and its correlation with the hindered dissolution process. *Hydrometallurgy* **2012**, *111–112*, 114–123. [CrossRef]
5. Wei, Z.; Li, Y.; Xiao, Q.; Song, S. The influence of impurity monovalent cations adsorption on reconstructed chalcopyrite (001)-s surface in leaching process. *Minerals* **2016**, *6*, 89. [CrossRef]
6. Li, Y.; Kawashima, N.; Li, J.; Chandra, A.P.; Gerson, A.R. A review of the structure, and fundamental mechanisms and kinetics of the leaching of chalcopyrite. *Adv. Colloid Interface Sci.* **2013**, *197–198*, 1–32. [CrossRef] [PubMed]
7. Córdoba, E.M.; Muñoz, J.A.; Blázquez, M.L.; González, F.; Ballester, A. Leaching of chalcopyrite with ferric ion. Part I: General aspects. *Hydrometallurgy* **2008**, *93*, 81–87. [CrossRef]

8. Sinha, M.K.; Sahu, S.K.; Pramanik, S.; Prasad, L.B.; Pandey, B.D. Recovery of high value copper and zinc oxide powder from waste brass pickle liquor by solvent extraction. *Hydrometallurgy* **2016**, *165*, 182–190. [CrossRef]
9. Cheng, C.Y.; Barnard, K.R.; Zhang, W.; Zhu, Z.; Pranolo, Y. Recovery of nickel, cobalt, copper and zinc in sulphate and chloride solutions using synergistic solvent extraction. *Chin. J. Chem. Eng.* **2016**, *24*, 237–248. [CrossRef]
10. Shahcheraghi, S.H.; Khayati, G.R.; Ranjbar, M. Improved dynamic modeling and simulation of an industrial copper solvent extraction process. *Hydrometallurgy* **2016**. [CrossRef]
11. Devi, N. Solvent extraction and separation of copper from base metals using bifunctional ionic liquid from sulfate medium. *Trans. Nonferrous Met. Soc. China* **2016**, *26*, 874–881. [CrossRef]
12. Karnib, M.; Kabbani, A.; Holail, H.; Olama, Z. Heavy metals removal using activated carbon, silica and silica activated carbon composite. *Energy Procedia* **2014**, *50*, 113–120. [CrossRef]
13. Sheet, I.; Kabbani, A.; Holail, H. Removal of heavy metals using nanostructured graphite oxide, silica nanoparticles and silica/graphite oxide composite. *Energy Procedia* **2014**, *50*, 130–138. [CrossRef]
14. El-Bahy, S.M.; El-Bahy, Z.M. Synthesis and characterization of polyamidoxime chelating resin for adsorption of Cu(II), Mn(II) and Ni(II) by batch and column study. *J. Environ. Chem. Eng.* **2016**, *4*, 276–286. [CrossRef]
15. Mukherjee, R.; Bhunia, P.; De, S. Impact of graphene oxide on removal of heavy metals using mixed matrix membrane. *Chem. Eng. J.* **2016**, *292*, 284–297. [CrossRef]
16. Bowden, L.I.; Johnson, K.L.; Jarvis, A.P.; Robinson, H.; Ghazireh, N.; Younger, P.L. The use of Basic Oxygen Steel Furnace Slag (BOS) as a High Surface Area Media for the Removal of Iron from Circumneutral Mine Waters. In Proceedings of the 7th International Conference on Acid Rock Drainage (ICARD), St. Louis, MO, USA, 26–30 March 2006; pp. 25–30.
17. Name, T.; Sheridan, C. Remediation of acid mine drainage using metallurgical slags. *Miner. Eng.* **2014**, *64*, 15–22. [CrossRef]
18. Kruse, N.; Mackey, A.; Bowman, J.; Brewster, K.; Riefler, R.G. Alkalinity production as an indicator of failure in steel slag leach beds treating acid mine drainage. *Environ. Earth Sci.* **2012**, *67*, 1389–1395. [CrossRef]
19. Deepatana, A.; Valix, M. Recovery of nickel and cobalt from organic acid complexes: Adsorption mechanisms of metal-organic complexes onto aminophosphonate chelating resin. *J. Hazard. Mater.* **2006**, *137*, 925–933. [CrossRef] [PubMed]
20. Shukla, S.; Pai, R.S.; Shendarkar, A.D. Adsorption of Ni(II), Zn(II) and Fe(II) on modified coir fibres. *Separat. Purif. Technol.* **2006**, *47*, 141–147. [CrossRef]
21. Pramanik, S.; Dhara, P.K.; Chattopadhyay, P. A chelating resin containing bis(2-benzimidazolylmethyl) amine: Synthesis and metal-ion uptake properties suitable for analytical application. *Talanta* **2004**, *63*, 485–490. [CrossRef] [PubMed]
22. Jing, X.; Liu, F.; Yang, X.; Ling, P.; Li, L.; Long, C.; Li, A. Adsorption performances and mechanisms of the newly synthesized N,N′-di(carboxymethyl) dithiocarbamate chelating resin toward divalent heavy metal ions from aqueous media. *J. Hazard. Mater.* **2009**, *167*, 589–596. [CrossRef] [PubMed]
23. Li, W.; Zhao, H.; Teasdale, P.; John, R.; Zhang, S. Synthesis and characterisation of a polyacrylamide-polyacrylic acid copolymer hydrogel for environmental analysis of Cu and Cd. *React. Funct. Polym.* **2002**, *52*, 31–41. [CrossRef]
24. Dakova, I.; Karadjova, I.; Ivanov, I.; Georgieva, V.; Evtimova, B.; Georgiev, G. Solid phase selective separation and preconcentration of Cu(II) by Cu(II)-imprinted polymethacrylic microbeads. *Anal. Chim. Acta* **2007**, *584*, 196–203. [CrossRef] [PubMed]
25. Liu, Y.; Chang, X.; Yang, D.; Guo, Y.; Meng, S. Highly selective determination of inorganic mercury (II) after preconcentration with Hg(II)-imprinted diazoaminobenzene-vinylpyridine copolymers. *Anal. Chim. Acta* **2005**, *538*, 85–91. [CrossRef]
26. Bao, Y.; Yuan, F.; Zhao, X.; Liu, Q.; Gao, Y. Equilibrium and kinetic studies on the adsorption debittering process of ponkan (citrus reticulata blanco) juice using macroporous resins. *Food Bioprod. Process.* **2015**, *94*, 199–207. [CrossRef]
27. Liu, Y.; Di, D.; Bai, Q.; Li, J.; Chen, Z.; Lou, S.; Ye, H. Preparative separation and purification of rebaudioside a from steviol glycosides using mixed-mode macroporous adsorption resins. *J. Agric. Food Chem.* **2011**, *59*, 9629–9636. [CrossRef] [PubMed]

28. Namasivayam, C.; Kadirvelu, K. Uptake of mercury(II) from wastewater by activated carbon from an unwanted agricultural solid by-product: Coirpith. *Carbon* **1999**, *37*, 79–84. [CrossRef]
29. Ho, Y.S.; McKay, G. Kinetic models for the sorption of dye from aqueous solution by wood. *Process Saf. Environ. Prot.* **1998**, *76*, 183–191. [CrossRef]
30. Yeddou, N.; Bensmaili, A. Kinetic models for the sorption of dye from aqueous solution by clay-wood sawdust mixture. *Desalination* **2005**, *185*, 499–508. [CrossRef]
31. Zhang, Y.L.; Yu, X.J.; Wang, Q.L.; Jiang, Z.J.; Fang, T. Adsorption of zinc onto anionic ion-exchange resin from cyanide barren solution. *Chin. J. Chem. Eng.* **2015**, *23*, 646–651. [CrossRef]
32. Doğan, M.; Abak, H.; Alkan, M. Adsorption of methylene blue onto hazelnut shell: Kinetics, mechanism and activation parameters. *J. Hazard. Mater.* **2009**, *164*, 172–181. [CrossRef] [PubMed]
33. Chen, C.-Y.; Chiang, C.-L.; Chen, C.-R. Removal of heavy metal ions by a chelating resin containing glycine as chelating groups. *Separat. Purif. Technol.* **2007**, *54*, 396–403. [CrossRef]
34. Al-Muallem, H.A.; Wazeer, M.I.M.; Ali, S.A. Synthesis and solution properties of a new pH-responsive polymer containing amino acid residues. *Polymer* **2002**, *43*, 4285–4295. [CrossRef]
35. Lee, W.; Lee, S.-E.; Lee, C.-H.; Kim, Y.-S.; Lee, Y.-I. A chelating resin containing 1-(2-thiazolylazo)-2-naphthol as the functional group; synthesis and sorption behavior for trace metal ions. *Microchem. J.* **2001**, *70*, 195–203. [CrossRef]
36. Gupta, A.P.; Varshney, P.K. Studies on tetracycline hydrochloride sorbed zirconium tungstophosphate; La(III)-selective chelating ion exchanger. *React. Funct. Polym.* **1996**, *31*, 111–116. [CrossRef]